Journal of Photochemistry and Photobiology A: Chemistry 353 (2018) 349–357

Contents lists available at ScienceDirect

Journal of Photochemistry and Photobiology A: Chemistry

journal homepage: www.elsevier.com/locate/jphotochem

Photophysical characterization of hydroxy and ethoxy phenalenone derivatives

C. Sandoval-Altamirano[a], J.R. De la Fuente[a], E. Berrios[a], S.A. Sanchez[b], N. Pizarro[c], J. Morales[d], G. Gunther[a,*]

[a] Universidad de Chile, Facultad de Ciencias Químicas y Farmacéuticas, Departamento de Química Orgánica y Fisicoquímica, Casilla 233, Santiago 1, Chile
[b] Universidad de Concepción, Facultad de Ciencias Químicas, Departamento de Polímeros, Concepción, Chile
[c] Universidad Andrés Bello, Facultad de Ciencias Exactas, Departamento de Ciencias Químicas, Quillota 980, Viña del Mar, Chile
[d] Universidad de Chile, Facultad de Ciencias Químicas y Farmacéuticas, Departamento de Ciencias y Tecnología Farmacéutica, Santiago, Chile

ARTICLE INFO

Article history:
Received 6 November 2017
Received in revised form 27 November 2017
Accepted 28 November 2017
Available online 2 December 2017

Keywords:
Phenlenone
Phenalenone derivatives
Singlet Oxygen

ABSTRACT

Phenalenone has been extensively studied due to its photophysical behavior. However, fewer are the articles referring to the phenalenone derivatives as singlet oxygen generators. The incorporation of substituents on the phenalenone ring rearranges the molecular electronic states changing its photophysical behavior. In order to rationalize the effect of the presence of electron-donor substituents on the phenalenone ring, we studied two ethoxy derivatives and their corresponding hydroxyl precursors. All derivatives prepared present smaller singlet oxygen quantum yield values than phenalenone. These lower quantum yields can be rationalized by considering non-radiative decay of singlet excited state absent in unsubstituted phenalenone. The hydroxy and alkoxy derivatives substituted in position 6 of phenalenone have larger fluorescence quantum yields than the ones substituted in position 3. Interestingly, 3-hydroxy-phenalenone shows a low emission quantum yield with two emission bands, which can be related with equilibria between diketo and enol tautomers in the first excited singlet state. Flash photolysis spectra for all derivatives were measured and the extinction coefficients of triplet–triplet absorption were evaluated near 500 nm.

1. Introduction

Phenalenone (perinaphthenone, 1H-phenalen-1-one), an aromatic ketone, has been widely used as a singlet oxygen sensitizer in photochemistry and photobiology [1]. With singlet oxygen quantum yields close to unity in most solvents, it has been proposed as universal reference [1,2]. Phenalenone derivatives are found in plants and fruits [3,4]. Phenyl-phenalen-1-one derivatives present in plant extracts are potent antifungal phytoalexins [5], and they play a role in the protection against pathogens through photosensitization processes involving singlet oxygen participation [6,7]. Phenalenone hydroxylated derivatives have been employed as chromophore model of haemocorin, a colored dihydroxy phenalenone found in Australian plants [8,9]. Recently, the phenalenone skeleton with hydroxy substituents has been obtained from the rearrangement of dinaphtyl ketones in acid media [10].

The presence of an α,β-unsaturated carbonyl group in this compound, is the main responsible of its remarkable photophysical and photochemical properties. The nature of the lowest singlet and triplet excited states of aromatic ketones (electronic configurations $n\pi^*$ or $\pi\pi^*$), is highly dependent on the interaction between the carbonyl group and the arene system (including the substituents present) [11].

The presence of electron-acceptor or electron-donor substituents on phenalenone derivatives are responsible for the higher sensitivity of the electronic states to the polarity of the local environment. Thus, the spectroscopic behavior of these molecules is highly susceptible to the physical chemical properties of the environment [12]. Phenalenone (**PN**) has been described as a photo-stable compound in several solvents, like benzene or hexane, but its triplet excited state can abstract a proton in alcohols with low photo-reduction quantum yields [13], and in dimethylformamide or 1,4-dioxane also photo-decompose [11]. Phenalenone and 6-hydroxyphenalenone are known to yield photo-generated radicals in basic propanol [14].

We are interested in the design of photosensitizers based on the phenalenone chromophore considering their potential

* Corresponding author.
E-mail address: ggunther@ciq.uchile.cl (G. Gunther).

https://doi.org/10.1016/j.jphotochem.2017.11.049
1010-6030/

applications as singlet oxygen generators. Then, our aim is the use of these derivatives as a group capable of generating singlet oxygen, linked to specific moieties which would allow their recognition or preferential localization in lipid membranes, and hence promoting damage at specific locations. Keeping this in mind, in this article we report the photophysical characterization of two ethoxy derivatives and their hydroxyl precursors (modified in position 3 and 6, Fig. 1). We choose these substituents because will be the linkers in subsequent derivatizations. The photophysical characterization of the aforementioned compounds (the simplest alkoxy derivatized molecules) has been poorly reported. Our results showed that the presence of ethoxy groups decreased the capability of the molecule to generate singlet oxygen. Additionally, the 3- derivatives showed low fluorescence and in the case of hydroxy derivative, two emission bands were observed in some solvents. Moreover, fluorescence quantum yields of 6-substituted derivatives were higher than the values for 3-substituted ones with the concomitant reduction in singlet oxygen generation quantum yield, parameter which was also determined in several solvents.

2. Experimental section

2.1. Synthesis of 6-hydroxyphenalenone (6OHPN)

For this synthesis, the protocol published by Cook et al. [8] and Otalvaro et al. [15] was used. Briefly, a mixture of 2,7-dihydroxynaphthalene (2 g), sodium-nitrobenzenesulphonate (2.5 g), glycerol (5 g), phosphoric acid (98%; 12 LC.), ferrous sulphate (0.6 g) and boric acid (1 g) was heated during 10 min to 150 °C and then maintained at 150–170 °C for 35 min. The mixture was then poured into water, warmed to coagulate the precipitate, and filtered. The residue was washed with water and then extracted with hot aqueous sodium carbonate. The magenta colored filtrate was acidified with hydrochloric acid and the precipitate was collected, washed with water, and dried. Column chromatography was performed with chloroform:ethanol (10:1) as mobile phase to obtain pure 6-hydroxyphenalenone.

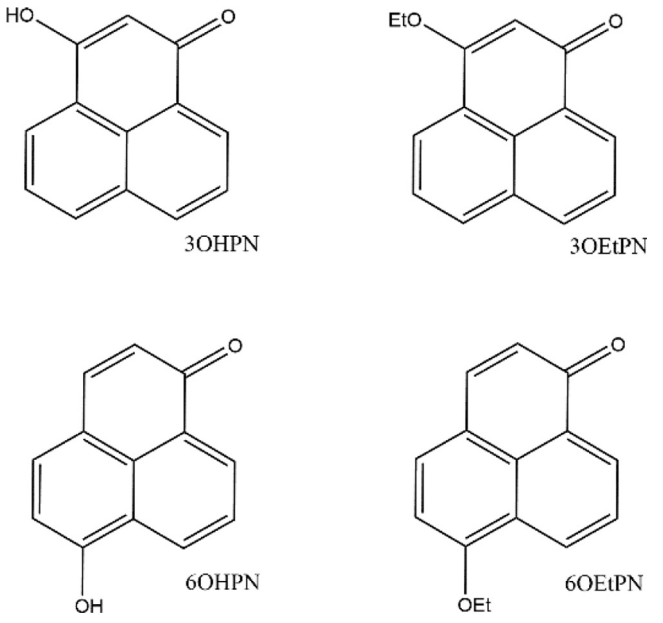

Fig. 1. Chemical structure of 3- and 6-hydroxyphenalenones and the corresponding ethoxy derivatives (**OHPNs** and **OEtPNs**).

2.2. Synthesis of 3-hydroxyphenalenone (3OHPN)

The protocol from Eistert at al. [16] was employed. Briefly, 7.5 g (0.038 mol) of powdered naphthalic anhydride were added to a three-necked flask containing 30 mL of diethyl malonate. When homogeneous slurry was formed 7.50 g (0.055 mol) of water-free zinc chloride were added. The mixture was heated under stirring for 3 h at 145–155 °C and then held for 6 h at this temperature. Solid dark crude was crushed, treated with hot water, solubilized with ammonia 10% in water and precipitated with acetic acid. Column chromatography was performed with chloroform:ethanol (10:1) as mobile phase to obtain pure 3-hydroxyphenalenone.

2.3. Synthesis of 6-ethoxyphenalenone (6OEtPN)

200 mg of **6OHPN** (1 mmol) and 350 mg of anhydrous K_2CO_3 (2.5 mmol) were added to 15 mL of dry dimethylformamide (DMF), at room temperature 160 μL of Iodoethane (2 mmol) were added dropwise. After three hours, reaction mixture was extracted with ethyl ether and recrystallized from ethanol.

2.4. Synthesis of 3-ethoxyphenalenone (3OEtPN)

200 mg of **3OHPN** (1 mmol) were added to 70 mg of NaH (3 mmol) suspended in 15 mL of dry DMF and 160 μL of Iodoethane (2 mmol) were added dropwise at room temperature. After six hours, reaction mixture was extracted with ethyl ether and purified by column chromatography (chloroform was employed as mobile phase). A small amount of 2-ethyl-3-etoxyphenalenone was obtained as secondary product.

All solvents were HPLC or spectroscopic quality, reagents were analytical grade and employed with no further purification unless otherwise stated.

H NMR data of all synthesized products are shown in Supplementary data section.

2.5. Spectroscopic and photophysical measurements

UV–vis spectra were recorded on an Agilent 8453 Diode-Array spectrophotometer in the range of 250–700 nm. Emission spectra were measured in an ISS PC1 spectrofluorometer or a FluoroMax 4CP (Horiba Jovin Yvon) at room temperature or in EtOH/MeOH glass (4:1 v/v) at 77 K. Luminescence lifetime measurements were carried out with the time correlated single photon counting (TCSPC) method using a PicoQuant FluoTime 200 fluorescence lifetime spectrometer with a multichannel scaler (PicoQuant's Timeharp 250), or a PicoQuant FluoTime 300 fluorescence lifetime. As excitation source LEDs or lasers of adequate wavelength were employed. Fluorescence quantum yields were measured in a FluoroMax 4CP (Horiba Jovin Yvon) spectrofluorometer equipped with the Quanta-Phi integrating sphere.

Singlet oxygen, $O_2(^1\Delta_g)$, lifetime decays were acquired with a FluoTime 200 consisting in a multichannel scaler Nanoharp 200. Excitation at 355 nm was achieved with a laser FTSS355-Q3, (Crystal Laser, Berlin, Germany) working at 1 kHz repetition rate. For the detection at 1270 nm a NIR PMT H10330A (Hamamatsu) was employed. The $O_2(^1\Delta_g)$ quantum yields (Φ_Δ) were determined by comparing the intensity at zero time of the 1270 nm signals to those of optically-matched solutions of phenalenone as reference [2].

Nanosecond laser flash photolysis experiments were performed on Argon saturated acetonitrile (ACN) solutions by exciting at 355 nm and sweeping the absorption spectra between 300 and 750 nm. The instrument was described previously [17], some additional accessories are now available: excitation with a Continuum Surelite I 10 Hz Q-switched Nd-YAG laser, signal

collection with a WaveSurfer 600 MHz LeCroy oscilloscope. Software written in National Instrument LabView 8.0 [18] controls the laser, monochromator and shutters. Captured data are fed to an Igor Pro 6.3 [19] written program for treatment and display.

Theoretical calculations for **3OHPN** and **6OHPN** absorption spectra (vertical transition energies and oscillator strengths) in acetonitrile (ACN), benzene (BNZ), chloroform (CHL) and methanol (MET) were calculated using time-dependent DFT theory (TDDFT). All geometries were optimized using PBE0 [20] hybrid functional with def2-TZVP [21] as basis set for all atoms. The resolution-of-identity (RI) [22,23] approximation for Coulomb integrals was always applied plus auxiliary basis set [24]. The nature of the stationary points in the potential energy surface was characterized by normal mode analysis. Solvent effects were accounted for implicitly using the conductor-like screening model [25] (COSMO) with default parameters for all solvents. The keto-enol tautomerism for **3OHPN** between diketo and ketoenol forms was studied in vacuum at the PBE0/def2-TZVP level, in order to estimate its energy barrier. An initial guess for the transition state (TS) structure was calculated using the woelfling [26] module, a chain-of-states method, implemented in TURBOMOLE. The minimum energy path was discretized using 18 intermediate geometries. Then, this geometry was optimized along the normal mode with negative curvature to calculate a better approximation to the TS. Finally, a dynamic reaction coordinate calculation was carried out to ensure that the TS connects reactants to products. This was done using DRC [27] module. This module calculates a dynamic reaction coordinate solving Newton's equations on the Born-Oppenheimer potential energy surface on-the-fly as the molecule relaxes from the TS. The starting structures for backward and forward trajectories are generated distorting the TS geometry along the normal mode with imaginary frequency. Also, the starting nuclear kinetic energy is set equal to zero. All calculations were performed using TURBOMOLE [28] software.

3. Results and discussion

3.1. i. Steady state absorption and emission spectra

Fig. 2 shows the absorption spectra of **PN** and **PN** derivatives in ACN, those with substitution in position 3, show a similar shape to unsubstituted **PN** absorption, a group of bands between 300 and 360 nm and a second less intense band between 360 and 430 nm. The absorption spectra of these **PN** derivatives only differ from **PN** in the relative intensity (extinction coefficients) of the absorption bands. On the other hand, the absorption spectra of 6-substituted

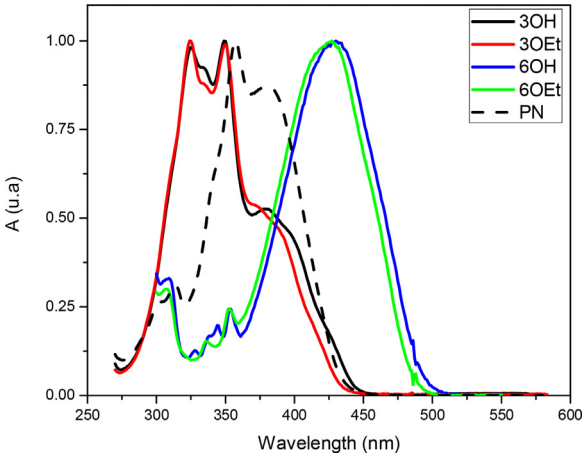

Fig. 2. Normalized absorption spectra of **PN** and **PN** derivatives in spectroscopic ACN.

PN and **PN** show noticeable differences. The absorption band located between 300 and 360 nm was weaker in these derivatives as compared with unsubstituted **PN**, and the second band (430 nm) was displaced to longer wavelength. The molar extinction coefficients determined for all derivatives in several solvents are shown in Table 1, and for both, 3 and 6 derivatives, the ethoxylated ones have larger extinction coefficients.

Normalized emission spectra of PN derivatives in ACN are shown in Fig. 3A. Emission intensity of the 3-substituted PN derivatives was lower than that observed for the 6-derivatives, in the case of **3OEtPN** almost negligible. Fluorescence quantum yields measured under air (Φ_{FL}) and under Argon ($\Phi_{FL,Ar}$) for 6-substituted derivatives are shown in Table 2. The similarity of the values indicates that oxygen does not quench appreciably the singlet states of these PN derivatives. Fluorescence quantum yields for **3-derivatives** were not evaluated because their low magnitudes and the significant overlap between the absorption an emission spectra, which would give rise to an important error by inner filter effect.

Although, **3OHPN** shows low emission intensity, it presented a singular behavior in MET and CHL, but not in BNZ or ACN (see Fig. 3B). In MET and CHL, two groups of bands centered at 380 nm and 480–520 nm are observed even at low concentration (emission spectrum shape does not depend on concentration if inner filter correction is made). This observations allow to discard a possible excimer formation in MET or CHL. On the other hand, uncorrected excitation spectrum in MET matches the absorption spectrum at all concentrations. Thus, the presence of emissive impurities can be also disregarded (Data shown in Fig. S5A).

Moreover, the 480–520 nm band shows solvatochromic effect, indicating a $n\pi^*$character, while the bands at 380 nm, that do not shift considerably, would have $\pi\pi^*$ character. This behavior may be caused by the existence of two states with different symmetry and low overlap or in the existence of two different minima on the same potential energy surface, as described for other systems where tautomeric equilibria exists [29–31]. It must be highlighted that for fluorophores derived from 2-phenalenone (benxozazolyl, benzothiazolyl and benzimidazolyl derivatives), two different emission bands have been reported, but their origin was attributed to the existence of two isolated and independent chromophor/fluorophor systems [12].

Low temperature emission measurements (Fig. 4) performed in glass (Ethanol:Methanol 4:1) at 77 K for all four **PN** derivatives displayed emission with: higher intensity,vibrational resolution, and a small hypsochromic shift (related to the emission spectra at room temperature). Only in the case of **3OEtPN** (despite its very low emission at room temperature, Fig. 4C) a small new group of bands centered around 600 nm appeared. These bands, could be ascribed to the phosphorescence coming from the triplet state. Flors et al. reported phosphorescence for unsubstituted phenalenone in glass, centered at 650 nm [32]. Thus, the presence of an ethoxy group in position 3 increases slightly the energy of triplet state with respect to unsubstituted PN triplet excited state. No emission from triplet states was detected neither for the hydroxy

Table 1
Molar extinction coefficients (ε, $\mathbf{10^3}\,M^{-1}\,cm^{-1}$) of phenalenone derivatives. Standard error for the data was below 6%.

Solvent	3OHPN	3OEtPN	6OHPN	6OEtPN
	ε (λ_{max}/nm)	ε (λ_{max}/nm)	ε (λ_{max}/nm)	ε (λ_{max}/nm)
Acetonitrile	9.0 (349)	12.7 (324)	5.8 (425)	9.7 (427)
Benzene	9.1 (334)	11.5 (351)	4.5 (428)	10.1 (422)
Chloroform	9.7 (333)	12.0 (328)	5.0 (440)	9.6 (433)
n-Hexane	n.e.	11.8 (347)	n.e.	9.8 (398)
Methanol	11.3 (338)	12.9 (328)	4.5 (455)	9.2 (436)

n.e., not evaluated.

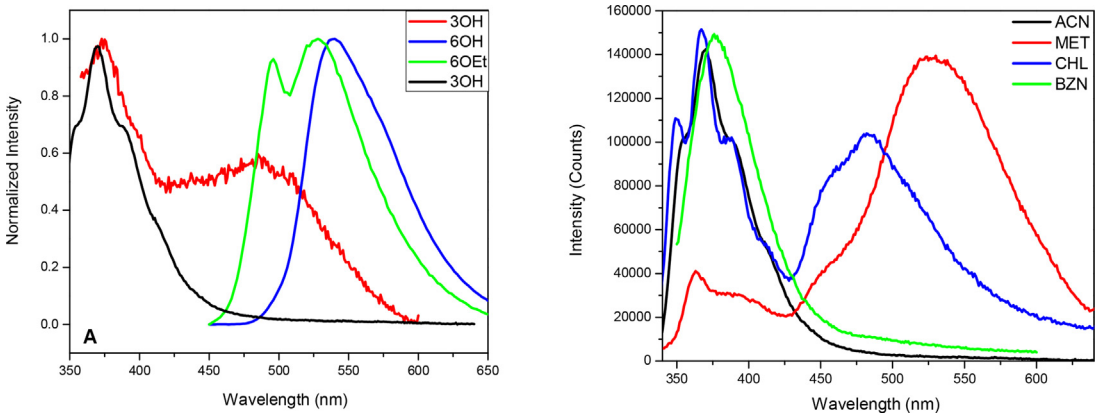

Fig. 3. A) Normalized emission of PN derivatives in ACN, for 3-PN derivatives λ_{ex} was 330 nm and for 6-PN derivatives 430 nm. B) Emission spectra of 3-hydroxyphenalenone (**3OHPN**) in several solvents, λ_{ex} = 330 nm.

Table 2
Fluorescence quantum yields of phenalenones derivatives.

Solvent	6OHPN		6EtOPN	
	Φ_{FL}	$\Phi_{FL,Ar}$	Φ_{FL}	$\Phi_{FL,Ar}$
Acetonitrile	0.027 ± 0.003	0.033 ± 0.002	0.018 ± 0.001	0.021 ± 0.003
Chloroform	0.202 ± 0.016	0.147 ± 0.009	0.049 ± 0.003	0.067 ± 0.004
Methanol	0.202 ± 0.013	0.167 ± 0.011	0.326 ± 0.028	0.304 ± 0.032

derivatives nor for 6-ethoxy at 77 K. The two groups of emission bands observed for **3OHPN** at room temperature in MET are also observed with higher intensity in ethanol/methanol glass at 77 K, revealing that bimolecular processes are not involved.

3.2. ii. Time resolved measurements

Fluorescence lifetimes data were analyzed by global fitting of a set of decays acquired at different emission wavelengths. A representative data analysis showing a monoexponential fit for **6OHPN** in methanol is shown in Fig. 5. For the 6-derivatives, the replacement of hydroxyl group with an ethoxy moeity resulted in shorter lifetimes in all the solvents used (Table 3), probably due to the opening of non-radiative paths involving vibrational relaxation. In the case of ethoxy derivative, lifetimes range from hundreds of picoseconds in BNZ, to more than 8 ns in MET. In all cases, saturation of solution with Argon did not change significatively the lifetime values, however, in several cases a small diminution in lifetimes is observed. Data shown in Table 3.

For the 3-substituted derivatives, only **3OHPN** emission was measured, because **3EtOPN** displays low intensity. Time Resolved

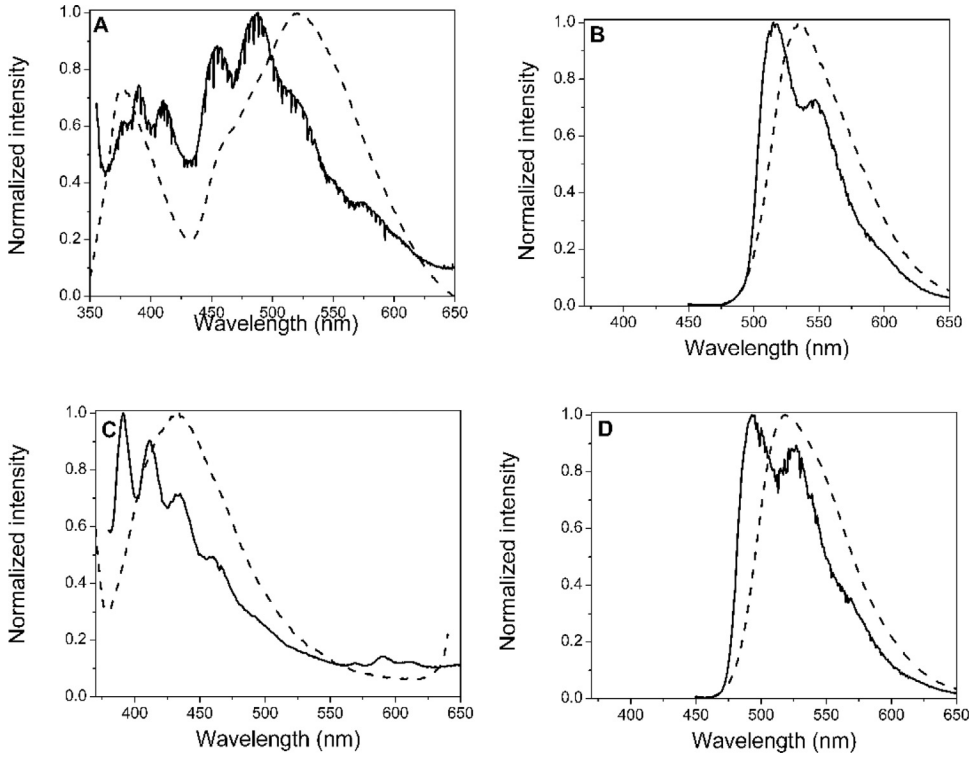

Fig. 4. Normalized low temperature emission spectra in ethanol:methanol (4:1) glass at 77 K, dashed lines correspond to emission at room temperature in the same solvent. A) **3OHPN** B) **6OHPN** C) **3OEtPN** D) **6OEtPN**.

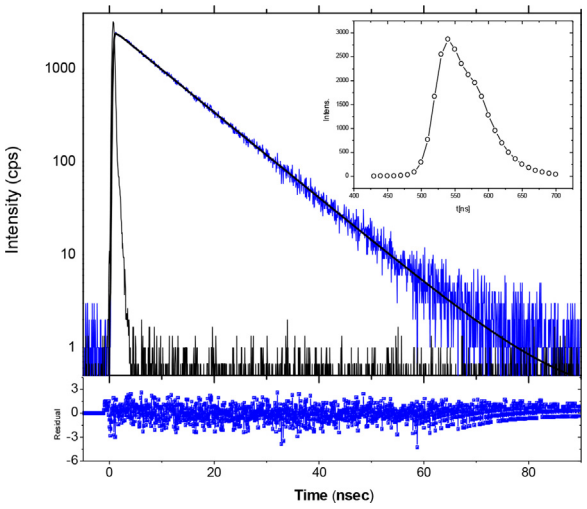

Fig. 5. Emission decay of **6OHPN** in MET at 550 nm. Inset corresponds to Time Resolved Spectra (TRES) obtained with global fitting of 25 decays, measured between 450 and 700 nm λ_{ex} = 405 nm.

Table 3
Lifetimes of singlet excited states of studied derivatives in several solvents. **6EtOPN** and **6OHPN** were excited at 405 nm and followed at 520 nm. **3OHPN** was excited at 330 nm and two decays were fitted, at 375 and 500 nm. All lifetimes were obtained from fitting of at least 20 decays obtained in TRES mode. Standard error for the data is below 4%.

Solvent	6EtOPN		6OHPN		3OHPN			
	τ_{air}/ns	τ_{Ar}/ns	τ_{air}/ns	τ_{Ar}/ns	τ_{air}/ns		τ_{Ar}/ns	
Acetonitrile	0.54	0.44	3.13	3.10	1.79		1.81	
Benzene	0.18	0.14	3.39	1.67	2.26		2.41	
Chloroform	1.26	1.25	7.07	6.66	1.07	0.17	1.10	0.20
Methanol	8.64	8.43	9.08	9.13	1.65	0.22	1.70	0.20

Emission Spectrum (TRES) shows two emission bands when **3OHPN** is excited at 330 nm (Fig. S5B). The excited state of higher energy (emission centered around 375 nm) has a monoexponential decay with lifetime around 2 ns, while the lower energy (emission centered around 500 nm) has a monoexponential lifetime dependent on the solvent. These results, combined with the previously discussed, allow to discard the existence of a coupled system, as an excimer. Lifetimes of both emissive states show a slight dependence on air oxygen presence.

3.3. iii. Singlet oxygen generation

The concentration of $O_2(^1\Delta_g)$ is expected to rise and decay reflecting triplet pathway according Eq. (1):

$$[O_2(^1\Delta_g)](t) = [^3PN]_o \frac{\tau_\Delta \quad k_\Delta^{O_2}[O_2]}{\tau_T - \tau_\Delta k_d^T + k_\Delta^{O_2}[O_2]} \left(e^{-t/\tau_\Delta} - e^{-t/\tau_T}\right) \quad (1)$$

where $k_\Delta^{O2}[O_2]$ accounts for the encounters of triplet sensitizer with ground state molecular oxygen which yield of $O_2(^1\Delta_g)$, k_d^T corresponds to sensitizer triple state unimolecular deactivation and τ_T and $\tau\Delta$ refer to the lifetimes of the triplet states of the photosensitizer and of $O_2(^1\Delta_g)$, respectively.

In this case, the infrared emission of excited oxygen obeys the following equation Eq. (2):

$$I(t) = -A_1 e^{-t/\tau_T} + A_2 e^{-t/\tau_\Delta} \quad (2)$$

The empirical constants A_1 and A_2 contain instrumental factors, kinetic parameters and ground state oxygen and excited sensitizer concentrations [33,34]. Fig. 6 shows the experimental time dependence observed for $O_2(^1\Delta_g)$ phosphorescence at 1270 nm upon excitation of **3OHPN** in ethanol equilibrated with air at 355 nm. As can be seen, the signal satisfactorily fits to a bi-exponential function. An exponential growth of near of 220 ns, was assigned to the excited triplet state of this compound in air equilibrated ethanol compatible with a diffusional quenching rate constant by O_2 of triplet excited state, *vide infra*. The decay of 12.9 μs was assigned to $O_2(^1\Delta_g)$ lifetime, being this value similar to the one reported for τ_Δ in this solvent (around 13 to 15 μs) [35], indicating that **3OHPN** does not quench $O_2(^1\Delta_g)$ in this solvent and conditions. Similar infrared emission profiles were observed for the other measured derivatives.

As mentioned in the experimental section, $O_2(^1\Delta_g)$ quantum yields, $\Phi\Delta$, were determined in several solvents by comparing the initial $O_2(^1\Delta_g)$ intensity with matched standard photosensitizer of known $\Phi\Delta$. The results (Table 4) indicate that the medium highly modulates the capacity of the studied compounds to generate $O_2(^1\Delta_g)$. Therefore, it can be concluded that high quantum yields for $O_2(^1\Delta_g)$ generation are related with a $\pi\pi^*$ configuration for the lowest triplet state (for ketones, this state has been described as a very efficient singlet oxygen generator), while in non-polar solvents where quantum yield value is lower, supporting a $n\pi^*$ configuration (for ketones this configuration has been reported to have singlet oxygen quantum yields around 0.3) [36]. This behavior, clearly observed in hydroxy derivatives, is consistent with the reported effect of solvent polarity in the energy arrangement of involved states and possible mixing of them for these systems.

Summarizing, low fluorescence quantum yields, indicate that singlet excited state deactivation is controlled by non-radiative processes (ISC to triplet excited state or IC to singlet ground state). Hence, ISC shows dependence on solvent properties. The long lifetimes for triplet states (see below) allows us to directly relate Φ_Δ with ISC, assuming that ground state of molecular oxygen is able to quench most of the triplet excited states formed. For **6OHPN**, the lowest singlet oxygen quantum yield values were obtained in BZN and CHL. Particularly, in MET, hydrogen bonding interactions could promote a lowered ISC, as reported by Martinez et al. [37] for 9H-Fluoren-9-one. Moreover, this proposal is consistent with the higher fluorescence quantum yield and singlet excited state lifetime determined in this protic solvent, with the exception of **6EtOPN**.

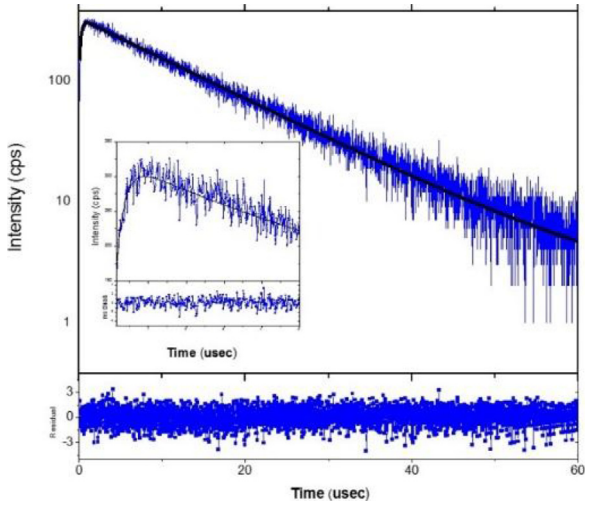

Fig. 6. Time resolved infrared emission of $O_2(^1\Delta_g)$ (1270 nm) obtained upon excitation of **3OHPN** at 355 nm in air-saturated ethanol. Inset corresponds to initial scale of decay, fitting residuals are given.

Table 4
$O_2(^1\Delta_g)$ quantum yields values for **PN** derivatives in several solvents, determined values are referred to phenalenone as actinometer, with excitation at 355 nm under air.

Solvent	Φ_Δ			
	3OHPN	3OEtPN	6OHPN	6OEtPN
Acetonitrile	0.833 ± 0.062	0.519 ± 0.021	0.657 ± 0.028	0.617 ± 0.025
Benzene	0.332 ± 0.012	0.735 ± 0.032	0.070 ± 0.010	0.861 ± 0.058
Chloroform	0.655 ± 0.027	–	0.161 ± 0.002	1.066 ± 0.085
Methanol	–	–	0.440 ± 0.010	0.670 ± 0.061

3.4. iv. Laser flash photolysis absorption experiments

Triplet-triplet absorption experiments in Argon saturated ACN solutions were performed for the four derivatives. The transient decays for both ethoxy derivatives were mono-exponential consistent with the absorption of only one species which is strongly quenched by oxygen. In fact, signal almost disappeared when oxygen was admitted to the samples. Also, the hydroxylated derivatives absorptions were totally quenched by oxygen, disappearing completely. Therefore, the observed transient absorptions should be attributed to the excited triplet state of the respective **PN** derivatives.

For the 3-substituted derivatives, Fig. 7, the transient spectra are similar showing four absorption bands and a ground depletion. For the **3OEtPN** maxima appear at 360, 400 and 510 nm with a lifetime of 9.2 +/− 0.06 μs, see inset in Fig. 7A, while the absorption at 750 nm shows a bi-exponential behavior with the shorter lifetime also of 9.2 μs. The ground depletion at 320 nm recovered with the same lifetime observed for absorptions at 360, 400 and 510 nm, therefore, an extinction coefficient $\varepsilon^T_{510nm} = 4210\ M^{-1}$ cm^{-1} at 510 nm was estimated for the triplet state. Estimation of ε cannot be done for the absorption bands below 500 nm due the ground state absorption extending from the UV to nearly 500 nm.

For the 3-hydroxy derivative, Fig. 7B, almost the same absorption peaks were observed showing a shift to the blue of ∼10 nm, with the ground depletion also at 320 nm. With this bleaching and the transient absorption, we estimated the molar absorptivity at 500 nm; $\varepsilon^T_{500nm} = 8425\ M^{-1}\ cm^{-1}$. Also in this case, it was not possible to estimate the extinction coefficient bellow 500 nm due the ground state absorption. It is interesting to note that for the 3-hydroxy derivative, the absorption band at 350 nm is larger than the one at 400 nm as compared with the **3OEtPN**, suggesting that this band is exacerbated by the —OH substitution.

For the **6OEtPN** derivative, Fig. 8A, the maxima appeared at 340 and 410 nm followed by a broad band with the maximum at 510 nm and a shoulder at 630 nm. Also, a bleaching at 380 nm was present. All these bands evolve monotonically with a lifetime of 9.8 ± 0.05 μs as shown in Fig. 8A inset. From the absorption data, we estimate a $\varepsilon^T_{510nm} = 7049\ M^{-1}\ cm^{-1}$.

For the **6OHPN** derivative, Fig. 8B, the transient spectra showed a very different behavior as compared with the **6OEtPN** derivative. Even if the positions of the maxima did not show appreciable change, several differences can be noticed: first, the decay at 340 nm is biexponential evidencing the formation of a long-lived transient decaying parallel to the decay at 390 nm after a delay of 10 μs, (Fig. 8B). This sharp absorption at 390 nm grew and decayed synchronously with the absorption appearing at 370 nm (not shown in the inset). These two absorptions at 370 and 390 nm grew with the same kinetic rate constant ($k = 3.1 \times 10^5\ s^{-1}$) than the decay of the absorption at 530 nm that clearly can be attributed to the triplet. Several separated experiments, using fresh solutions

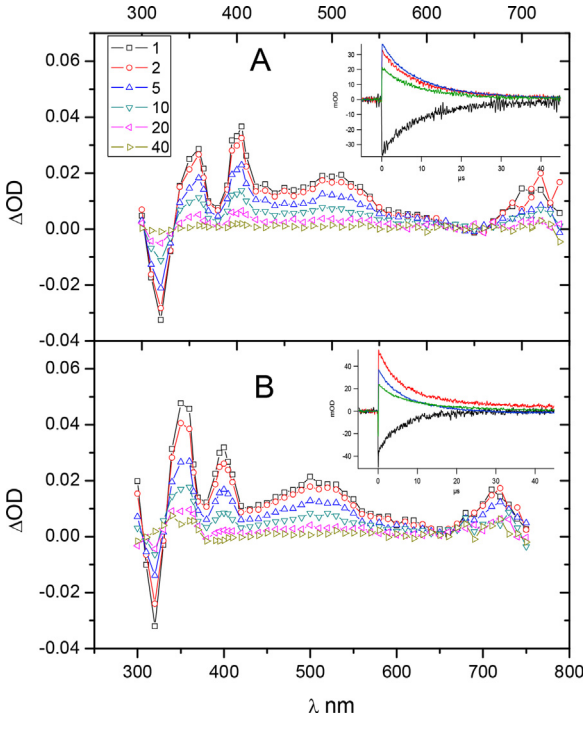

Fig. 7. Triplet-triplet absorption spectra for: A) **3OEtPN** substituted **PN** derivative. The inset shows the kinetic traces at: 320 (black), 360 (red), 400 (blue) and 510 nm (green), all of them of first kinetic order and a lifetime of 9.2 ± 0.06 μs. Panel B) contains the absorption transient spectra for the **3OHPN** derivative. Inset shows the decays at: 320 (black), 350 (red), 400 (blue) and 500 nm (green), all of them decay with a bi-exponential character. See text for explanations. (For interpretation of the references to colour in this figure legend, the reader is referred to the web version of this article.)

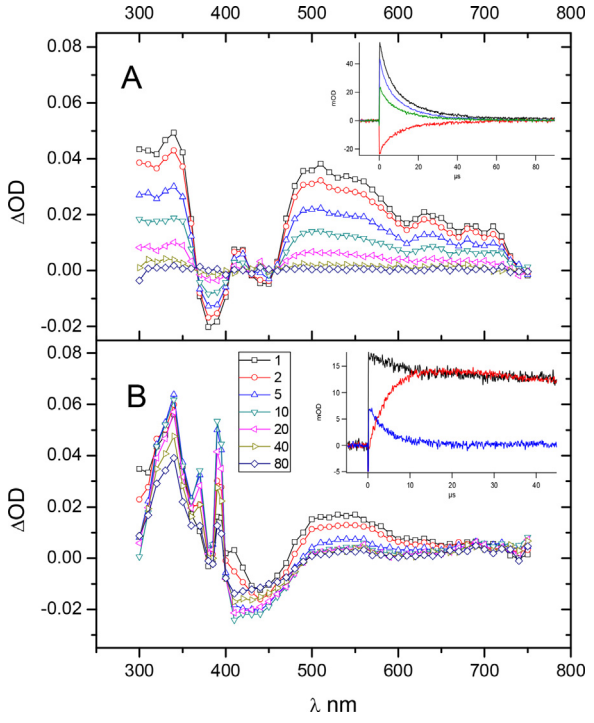

Fig. 8. Triplet-triplet absorption spectra for: A) 6 **OEtPN** derivative. Transient spectra show ground depletion at 380 nm useful for estimate the extinction coefficient for the triplet states. The inset shows the kinetic traces at: 340 (black), 380 (red), 510 (blue) and 630 nm (green), all of them mono-exponential with a lifetime of 9.8 ± 0.05 μs. Panel B) shows the transient spectra for the **6OHPN** derivative with maxima at 340, 360, 390 and 530 nm. The inset shows the kinetic behavior of a separated experiment at: 340 (black), 380 (red) and 530 nm (blue). See text for explanation. (For interpretation of the references to colour in this figure legend, the reader is referred to the web version of this article.)

measured at various wavelengths between 500 and 600 nm, allowed to measure a lifetime of 3.2 ± 0.04 μs for the excited triplet state of the **6OHPN** derivative. For this compound that not shows clear ground depletion, due to the growing of transient absorptions, it was not possible to estimate the extinction coefficient.

For both hydroxylated **PN,** some consumption was observed during the spectral and kinetic experiments. Therefore, it is likely that the estimated extinction coefficient for the **3OHPN** derivative was underestimated.

3.5. v. Theoretical calculations

To get deeper insight on the spectroscopic behavior of these systems, vertical electronic excitation spectra were theoretically predicted and compared with the experimental. Ground state equilibrium geometries for **6OHPN** and **3OHPN** were optimized in the ground state for ACN, MET, CHL and BNZ using COSMO model. The results (Table 5) showed four singlet low-lying excited states vertical transitions and oscillator strengths were obtained at the TDDFT level of theory at each S_0 equilibrium geometry. For **6OHPN** the main valence molecular orbitals involved in the S_0 to S_1 vertical excitation indicates that the electronic configuration corresponds to a $\pi \rightarrow \pi^*$ transition (Fig. S6, Supplementary information). On the other hand, S_2 shows an $n \rightarrow \pi^*$ character with negligible oscillator strength, as expected for such states in ketones. The next two singlet states, S_3 and S_4, have both $\pi \rightarrow \pi^*$ character and their oscillator strengths are approximately five times smaller than the corresponding value for S_1. Even though all singlet states in Table 4 are dominated by one singly-excited Slater determinant, S_3 and S_4 show increasing contributions from additional determinants compared to S_1 and S_2. For **3OHPN** the results showed (Table 4) that first vertical singlet transition is dipole allowed in ACN and MET, while forbidden in CHL and BNZ. However, the opposite is observed for S_2. The main character for S_1 and S_2 transitions in ACN and MET is $\pi \rightarrow \pi^*$ and $n \rightarrow \pi^*$, respectively. However, close energy degeneracy between these states probably mix their character. This assignment is reversed for S_1 and S_2 in CHL and BZN. Furthermore, S_1 vertical excitation energy is lowered by 0.07 eV and 0.122 eV in CHL and BZN, respectively as compared to ACN or MET (where no differences in energy were observed). S_2 and S_3 show $\pi \rightarrow \pi^*$ character and larger oscillator strengths than the same vertical transition in **6OHPN**.

Fig. 9 shows the simulated absorption spectra for **6OHPN** and **3OHPN** in ACN. For both molecules, TDDFT overestimated vertical transition energy by approximately 0.2 eV in average for all solvents (see Table 5). In order to plot Fig. 9, all transitions were broadened by a Gaussian function with standard deviation of ~14 nm. Despite of this rough approximation, there is an acceptable match between theoretical and experimental spectra. The simulated absorption spectrum for **3OHPN** suggests that there are three strong $\pi \rightarrow \pi^*$ vertical transitions above 300 nm (Table 5), while for **6OHPN** a strong $\pi \rightarrow \pi^*$ dominates over the next two singlet transitions with same character.

Theoretical studies on **PN** at the TDDFT [38] and DFT/MRCI [39] level, calculated the first four low-lying singlet states in vacuum. Both authors report that S_1 is $n \rightarrow \pi^*$ with no oscillator strength and S_2 to S_4 shows $\pi \rightarrow \pi^*$ character and nonzero oscillator strength. Nonetheless, no further discussion on the structure presented by the absorption spectrum of **PN** is provided.

In order to clarify the dual emission observed for **3OHPN** we explored the tautomeric equilibrium, where **3OHPN** can coexist with its β-diketone tautomer. Characterization through normal mode analysis showed only one imaginary frequency as expected (–2098 cm^{-1}). The inset in Fig. 10 depicts the transient state, TS, geometry showing O—H and C—H distances of 1.34 Å and 1.44 Å respectively, closely related to a TS geometry proposed for

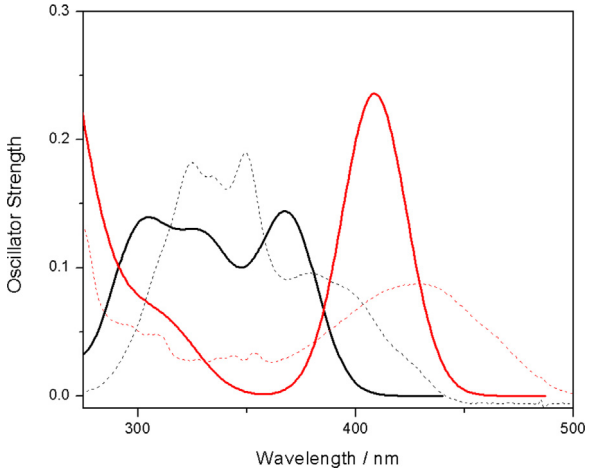

Fig. 9. Simulated absorption spectra for **6OHPN** (solid red) and **3OHPN** (solid black) in ACN at the RI-TDDFT PBE0/def2-TZVP COSMO level of theory. Dashed lines represent experimental absorption spectra in ACN (Fig. 2). Experimental absorption axis is not shown. (For interpretation of the references to colour in this figure legend, the reader is referred to the web version of this article.)

Table 5
Low-lying singlet–singlet vertical transitions, oscillator strengths and principal MO contributions (H for HOMO, L for LUMO) for **6OHPN** and **3OHPN** at RI-TDDFT PBE0/def2-TZVP COSMO level.

		6OHPN			3OHPN		
	Solvent	λ_{ex}/nm	Oscillator Strength	MO contributions	λ_{ex}/nm	Oscillator Strength	MO contributions
S_1	ACN	408	0.24	H to L (.95)	368	0.14	H to L (.86)
	MET	408	0.24	H to L (.95)	368	0.14	H to L (.86)
	CHL	402	0.24	H to L (.95)	377	0.00	H-2 to L (.96)
	BNZ	399	0.24	H to L (.95)	382	0.00	H-1 to L (.96)
S_2	ACN	378	0.00	H-1 to L (.96)	366	0.00	H-2 to L (.96)
	MET	378	0.00	H-1 to L (.96)	366	0.00	H-2 to L (.96)
	CHL	389	0.00	H-1 to L (.96)	367	0.15	H to L (.88)
	BNZ	395	0.00	H-1 to L (.96)	365	0.15	H to L (.89)
S_3	ACN	315	0.043	H-2 to L (.83)	331	0.11	H-1 to L (.83)
	MET	316	0.043	H-2 to L (.83)	331	0.11	H-1 to L (.83)
	CHL	313	0.034	H-2 to L (.81)	328	0.1	H-1 to L (.85)
	BNZ	312	0.031	H-2 to L (.80)	327	0.09	H-2 to L (.86)
S_4	ACN	292	0.049	H-3 to L (.76)	301	0.13	H-3 to L (.78)
	MET	292	0.049	H-3 to L (.76)	301	0.13	H-3 to L (.78)
	CHL	291	0.044	H-3 to L (.76)	300	0.12	H-3 to L (.76)
	BNZ	291	0.042	H-3 to L (.76)	299	0.11	H-3 to L (.76)

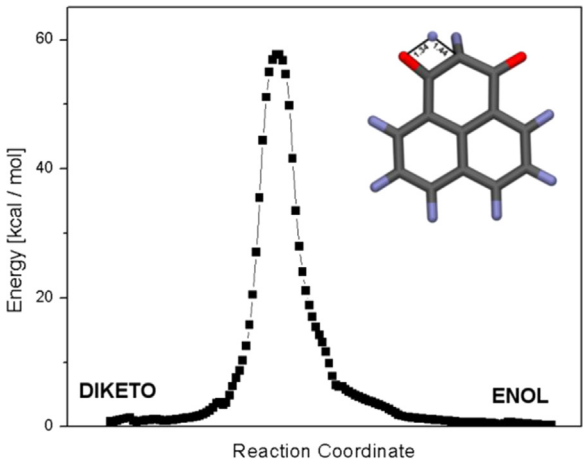

Fig. 10. DRC curve connecting **3OHPN** diketo and enol structures calculated at the RI-DFT PBE0/def2-TZVP level of theory. The inset shows the TS structure highlighting the distances (in Å) between the main atoms involved in the reaction.

cyclohexanedione tautomeric equilibrium [40]. To accept the TS structure is necessary to show that connects reactants to products. We used the DRC module in TURBOMOLE at the same level of theory than the TS search was performed. Fig. 10 shows the trajectory from reactant to product passing through the proposed TS. The diketo and enol form have approximately 1 kcal/mol energy difference at this level of theory, so no one is significantly favored in vacuum. Furthermore, the formation of the enol starting from the diketo requests surpassing a considerably energy barrier, 58.3 kcal/mol, which is in line with the one found for cyclohexanedione (63 kcal/mol) [40]. This high energy barrier could decrease by including explicit solvent effects; however, its value remains significant. [40] Therefore, in solution only one tautomeric form should prevail in the ground state agreeing with Fig. S6 B. One possible explanation to observe radiative relaxation of two different populations to the ground state is that in S_1 both tautomeric forms are separated by a smaller energy barrier so fast conversion from one form to the other is possible.

4. Conclusions

As consequence of this study, we can state that the presence of hydroxy and ethoxy substituents on the **PN** framework promotes significant changes on their photophysical properties and ground state behavior depending on the position of substituent, 6-substituted derivatives show higher emission quantum yields than 3-derivatives. Singlet excited state deactivation of these PN derivatives is mainly controlled by non-radiative processes: ISC to triplet excited state or IC to ground state singlet. **3OHPN**, despite its low emission efficiency, shows two emission bands in methanol and chloroform probably originated in the existence of a tautomeric equilibria in the first singlet excited state. Only **3OEtPN** shows detectable phosphorescence bands at 77 K, with a triplet excited state of higher energy than the one reported for phenalenone. Transients with triplet character were observed by flash photolysis for all derivatives studied, determining their lifetimes and exctintion coeficients. These phenalenone derivatives studied, have deactivation pathways that are not present in the unsubstituted phenalenone but still have significative singlet oxygen generation quantum yield, the most remarkable property of phenalenone.

Acknowledgements

This work was supported by funds from Fondecyt 1160705. Also, CS thanks DI (University of Chile), and SAS acknowledges Fondecyt 1140454.

The authors have declared that no conflicting interest exist.

Appendix A. Supplementary data

Supplementary data associated with this article can be found, in the online version, at https://doi.org/10.1016/j.jphotochem.2017.11.049.

References

[1] E. Oliveros, P. Suardimurasecco, T. Aminiansaghafi, A.M. Braun, H.J. Hansen, 1h-Phenalen-1-One – photophysical properties and singlet-Oxygen production, Helv. Chim. Acta 74 (1991) 79–90.
[2] R. Schmidt, C. Tanielian, R. Dunsbach, C. Wolff, Phenalenone, a universal reference compound for the determination of quantum yields of singlet oxygen sensitization, J. Photochem. Photobiol. A. 79 (1994) 11–17.
[3] J.G. Luis, F. Echeverri, W. Quinones, I. Brito, M. Lopez, F. Torres, G. Cardona, Z. Aguiar, C. Pelaez, M. Rojas, Irenolone and emenolone: two new types of phytoalexin from Musa paradisiaca, J. Org. Phys. 58 (1993) 4306–4308.
[4] D. Hölscher, S. Dhakshinamoorthy, T. Alexandrov, M. Becker, T. Bretschneider, A. Buerkert, A.C. Crecelius, D. De Waele, A. Elsen, D.G. Heckel, H. Heklau, C. Hertweck, M. Kai, K. Knop, C. Krafft, R.K. Maddula, C. Matthäus, J. Popp, B. Schneider, U.S. Schubert, R.A. Sikora, A. Svatoš, R.L. Swennen, Phenalenone-type phytoalexins mediate resistance of banana plants (Musa spp.) to the burrowing nematode Radopholus similis, Proc. Natl. Acad. Sci. U. S. A. 111 (2014) 105–110.
[5] J.R. Luque-Ortega, S. Martinez, J.M. Saugar, L.R. Izquierdo, T. Abad, J.G. Luis, J. Pinero, B. Valladares, L. Rivas, Fungus-elicited metabolites from plants as an enriched source for new leishmanicidal agents: antifungal phenyl-phenalenone phytoalexins from the banana plant (Musa acuminata) target mitochondria of Leishmania donovani promastigotes, Antimicrob. Agents Chemother. 48 (2004) 1534–1540.
[6] C. Flors, S. Nonell, Light and singlet oxygen in plant defense against pathogens: phototoxic phenalenone phytoalexins, Acc. Chem. Res. 39 (2006) 293–300.
[7] C. Flors, P.R. Ogilby, J.G. Luis, T.A. Grillo, L.R. Izquierdo, P.L. Gentili, L. Bussotti, S. Nonell, Phototoxic phytoalexins. Processes that compete with the photosensitized production of singlet oxygen by 9-phenylphenalenones, Photochem. Photobiol. 82 (2006) 95–103.
[8] R.G. Cooke, B.L. Johnson, W. Segal, Colouring matters of australian plants VI. haemocorin: the structure of the aglycone, Aust. J. Chem. 11 (1958) 230–233.
[9] R.G. Cooke, W. Segal, Colouring matters of australian plants V. haemocorin: the chemistry of the aglycone, Aust. J. Chem. 8 (1955) 413–421.
[10] S. Sasaki, E. Azuma, T. Sasamori, N. Tokitoh, K. Kuramochi, K. Tsubaki, Formation of phenalenone skeleton by an unusual rearrangement reaction, Org. Lett. 19 (18) (2017) 4846–4849.
[11] E. Oliveros, S.H. Bossmann, S. Nonell, C. Marti, G. Heit, G. Troscher, A. Neuner, C. Martinez, A.M. Braun, Photochemistry of the singlet oxygen [O-2((1)Delta(g))] sensitizer perinaphthenone (phenalenone) in N,N '-dimethylacetamide and 1,4-dioxane, New J. Chem. 23 (1999) 85–93.
[12] K.R. Phatangare, S.K. Lanke, N. Sekar, Phenalenone fluorophores-Synthesis, photophysical properties and DFT study, J. Fluoresc. 24 (2014) 1827–1840.
[13] H.H. Koller, G.P. Rabold, K. Weiss, T.K. Mukherjee, The Photochemistry of Phenalen-1-one, (1964) , pp. 332.
[14] G.P. Rabold, H.B.-E. Kedma, E. Reid, K. Weiss, Photochemically generated free radicals. I. The perinaphthenone system, J. Chem. Phys. 42 (1965) 2438–2447.
[15] F. Otalvaro, W. Quinones, F. Echeverri, B. Schneider, Synthesis of [phenyl-C-13 (6)]lachnanthocarpone and other C-13-labelled phenylphenalenones, J. Labelled Compd. Radiopharm. 47 (2004) 147–159.
[16] B. Eistert, W. Eifler, H. Goth, Versuche in der Reihe des 3-Hydroxy-1-0x0-phenalens und des 1.2.3-Trioxo-2.3-dihydro-phenalens, Chem. Ber. 101 (1968) 2162–2175.
[17] J.R. De la Fuente, Á. Cañete, C. Jullian, C. Saitz, C. Aliaga, Unexpected imidazoquinoxalinone annulation products in the photoinitiated reaction of substituted-3-Methyl-Quinoxalin-2-Ones with N-Phenylglycine, Photochem. Photobiol. 89 (2013) 1335–1345.
[18] LabVIEW, in, National Instruments Corporation, 2005.
[19] Igor Pro, in, Wavemetrics, 2006.
[20] C. Adamo, V. Barone, Toward reliable density functional methods without adjustable parameters: the PBE0 model, J. Chem. Phys. 110 (1999) 6158–6158.
[21] F. Weigend, R. Ahlrichs, Balanced basis sets of split valence, triple zeta valence and quadruple zeta valence quality for H to Rn: design and assessment of accuracy, Phys. Chem. Chem. Phys. 7 (2005) 3297–3297.
[22] K. Eichkorn, O. Treutler, H. Öhm, M. Häser, R. Ahlrichs, Auxiliary basis sets to approximate Coulomb potentials, Chem. Phys. Lett. 240 (1995) 283–290.

[23] K. Eichkorn, F. Weigend, O. Treutler, R. Ahlrichs, Auxiliary basis sets for main row atoms and transition metals and their use to approximate Coulomb potentials, Theor. Chem. Acc. 97 (1997) 119–124.
[24] F. Weigend, Accurate coulomb-fitting basis sets for H to Rn, Phys. Chem. Chem. Phys. 8 (2006) 1057–1057.
[25] A. Klamt, G. Schüürmann, COSMO: a new approach to dielectric screening in solvents with explicit expressions for the screening energy and its gradient, J. Chem. Soc., Perkin Trans. 2 (1993) 799–805.
[26] P. Plessow, Reaction path optimization without NEB springs or interpolation algorithms, J. Chem. Theory Comput. 9 (2013) 1305–1310.
[27] A. Hellweg, Heuristic control of kinetic energy in dynamic reaction coordinate calculations, J. Comput. Chem. 34 (2013) 1835–1841.
[28] TURBOMOLE V7.0 2015, a development of University of Karlsruhe and Forschungszentrum Karlsruhe GmbH, 1989–2007, TURBOMOLE GmbH, since 2007; available from http://www.turbomole.com, in.
[29] I.M. Craig, H.M. Duong, F. Wudl, B.J. Schwartz, A new route to dual fluorescence: spectroscopic properties of the valence tautomers of a 3-(2H)-isoquinolinone derivative, Chem. Phys. Lett. 477 (2009) 319–324.
[30] J.C. Germino, C.A. Barboza, F.J. Quites, P.A.M. Vazquez, T.D.Z. Atvars, Dual emissions of salicylidene-5-chloroaminepyridine due to excited state intramolecular proton transfer: dynamic photophysical and theoretical studies, J. Phys. Chem. C 119 (2015) 27666–27675.
[31] A.S. Klymchenko, C. Kenfack, G. Duportail, Y. Mély, Effects of polar protic solvents on dual emissions of 3-hydroxychromones, J. Chem. Sci. 119 (2007) 83–89.
[32] C. Flors, S. Nonell, On the phosphorescence of 1H-phenalen-1-one, Helv. Chim. Acta 84 (2001) 2533–2539.
[33] A. Jimenez-Banzo, X. Ragas, P. Kapusta, S. Nonell, Time-resolved methods in biophysics. 7. Photon counting vs. analog time-resolved singlet oxygen phosphorescence detection, Photochem. Photobiol. Sci. 7 (2008) 1003–1010.
[34] S. Nonell, S.E. Braslavsky, Time-resolved singlet oxygen detection, Method Enzymol. 319 (2000) 37–49.
[35] J.N. Chacon, J. Mclearie, R.S. Sinclair, Singlet oxygen yields and radical contributions in the dye-sensitized photo-oxidation in methanol of esters of poly-unsaturated fatty-Aacids (Oleic, linoleic linolenic and arachidonic), Photochem. Photobiol. 47 (1988) 647–656.
[36] R.W. Redmond, S.E. Braslavsky, Time-Resolved thermal lensing and phosphorescence studies on photosensitized singlet molecular-oxygen formation – influence of the electronic configuration of the sensitizer on sensitization efficiency, Chem. Phys. Lett. 148 (1988) 523–529.
[37] C.G. Martinez, A. Neumer, C. Marti, S. Nonell, A.M. Braun, E. Oliveros, Effect of the media on the quantum yield of singlet Oxygen ($O_2(^1\Delta_g)$) production by 9H-fluoren-9-one: solvents and solvent mixtures, Helv. Chim. Acta 86 (2003) 384–397.
[38] J. Arnbjerg, M.J. Paterson, C.B. Nielsen, M. Jørgensen, O. Christiansen, P.R. Ogilby, One- and two-Photon photosensitized singlet oxygen production: characterization of aromatic ketones as sensitizer standards, J. Phys. Chem. A 111 (2007) 5756–5767.
[39] M.C. Daza, M. Doerr, S. Salzmann, C.M. Marian, W. Thiel, Photophysics of phenalenone: quantum-mechanical investigation of singlet?triplet intersystem crossing, Phys. Chem. Chem. Phys. 11 (2009) 1688.
[40] G. Alagona, C. Ghio, Keto-enol tautomerism in linear and cyclic β-diketones: a DFT study in vacuo and in solution, Int. J. Quantum Chem. 108 (2008) 1840–1855.